Non-purged voltammetry explored with AGNES

D. Aguilar[a], J. Galceran[a *], E. Companys[a], J. Puy[a], C. Parat[b], L. Authier[b], M. Potin-Gautier[b]

[a]Departament de Química. Universitat de Lleida and AGROTECNIO, Rovira Roure 191, 25198 Lleida, Catalonia, Spain

[b]Université de Pau et des Pays de l'Adour, L.C.A.B.I.E, UMR 5254, IPREM, Avenue Pierre Angot, 64053 Pau Cedex 9, France

*corresponding author galceran@quimica.udl.cat

Abstract

The reduction of oxygen increases pH in the surroundings of an electrode. A theoretical model estimates the steady-state pH profile from the surface of the electrode up to the bulk solution. A very simple formula predicts that, in non-deareated solutions, for bulk pH-values between 4.0 and 10.0, the corresponding surface pH could be as high as 10.3, regardless of the thickness of the diffusion layer and composition of the sample (except if it has a buffering capacity). For bulk pH lower than 3.0 or higher than 10, pH increases are negligible. Less steep pH-profiles are obtained with buffers (such as MOPS 0.01 M or MES 0.01 M). The change in surface pH modifies the local speciation and hinders the standard interpretation of voltammetric responses. The electroanalytical technique Absence of Gradients and Nernstian Equilibrium Stripping (AGNES), implemented with Screen Printed Electrodes (SPE), provides experimental insights into this phenomenon. AGNES probes the free metal concentration at the electrode surface, from which the surface pH can be estimated for systems of known composition. These estimations agree with the theoretical model for the assayed systems. Additionally, the quantification of the bulk free Zn^{2+} and Cd^{2+} concentrations with specific modifications of AGNES for non-purged synthetic solutions is discussed. In general, more accurate determinations of the bulk free metal concentrations in non-purged solutions are

expected: i) when the calibration is performed in a medium where the pH increase induces similar changes in the surface free metal concentration and in the sample solution and ii) when the system is more buffered.

Keywords: deaeration, purge, dissolved oxygen, voltammetry, heavy metals, AGNES, deoxygenation, SPE

1. Introduction

Dissolved oxygen is considered a nuisance in voltammetry because it can be directly reduced to water via a four-electron reaction,

$$O_2 + 4H^+ + 4e^- \rightleftarrows 2H_2O \quad (1)$$

or to hydrogen peroxide [1] via a two-electron reaction,

$$O_2 + 2H^+ + 2e^- \rightleftarrows H_2O_2 \quad (2)$$

However, depending on the applied potential, the number of electrons accepted by oxygen could be a combination of the n_e=2 and n_e=4 pathways (reactions (1) and (2)) [2]. These reduction processes may cause two different types of interference [3]: i) By affecting the reading of the analytical signal against a large background current. This can lead to a reduced accuracy of the current of interest in natural waters where the dissolved oxygen concentration is much larger than those of trace metals (around 4-6 orders of magnitude). ii) The products of the reactions (1) and (2) can react with the analyte. The consumption of protons increases the pH at the electrode surface (pH^S) and can alter the local speciation (e.g. formation of soluble and insoluble species such as metal hydroxides). In previously published works, pH^S in non-deaerated solutions has

been estimated to be in the range 10 to 11 [4;5]. Micropositioned microelectrodes have been used in the literature to determine pH profiles [6;7].

Usual strategies to overcome the oxygen interference are: i) to add a pH buffer to the sample, which is not very recommended for ultratrace determinations because of possible contaminations; ii) the use of inert gases to eliminate the oxygen, which has been the most applied solution in voltammetry [8]. However, for *in situ* measurements, deaeration is inconvenient to perform (transport of N_2 bottles could be problematic) and may also lead to the elimination of CO_2 and, thus, to a high increase of the sample pH. Thus, the performance of non-purged experiments is a challenge and more insights are needed before *in situ* measurements can be performed with a sound interpretation. In fact, some authors have already demonstrated that it is possible to carry out measurements in solutions without removal of oxygen. For instance, Square-wave anodic Stripping voltammetry (SWASV) with relatively high frequency has been used to determine lead in rainwater [9] or background subtraction and the use of SWASV under appropriate conditions has been applied to trace metals in estuarine and coastal samples [10]. Cu has also been measured in non-purged seawater by pseudopolarography and a vibrating gold microwire electrode, because the metal reduction wave is at more positive potential than that for dissolved oxygen [11]. The large addition of sodium sulphite was also reported to spare the need of purging [12]. Stripping chronopotentiometry at scanned deposition potential (SSCP) in presence of oxygen has also been applied to study trace metal speciation [13]. Some of these experiments proceed in well buffered aquatic media, such as seawater, where the increase in pH^S is lower.

AGNES (Absence of Gradients and Nernstian Equilibrium Stripping) is a recently developed voltammetric technique that allows a direct determination of the free metal concentration in solution. AGNES has been applied and validated to the determination

of Pb, Cd and Zn in synthetic systems [14-22], wine [23;24], solutions containing humic acids [25;26], nanoparticles [27], quantum dots [28] and also natural waters (sea water [29] and river water [30]) in purged configurations.

In this work, we aim at: i) a better understanding of the impact of oxygen (at levels corresponding to equilibrium with atmosphere) on the local pH when a fixed potential for Zn or Cd deposition is prescribed at a mercury electrode, ii) show that AGNES can measure the free metal concentration at the electrode surface $[M^{2+}]^S$, which opens up the access to an experimental estimation of pH^S and iii) discuss the limits of the application of AGNES in non-purged solutions for the determination of the bulk free metal ion concentrations.

The outline is as follows. First, we gather experimental facts associated to the rise of pH in non-purged solutions in order to justify the essential assumptions of a simple theoretical model which allows estimating the surface pH and the concentration profiles of all relevant species. Then, in section 4, we discuss two phenomena that impact on AGNES application in non-purged solutions. In section 5, we use AGNES to measure $[M^{2+}]^S$ and pH^S and, in section 6, we discuss how AGNES can access to the free bulk concentration, $[M^{2+}]^*$, in non-purged solutions.

2. Experimental methods and materials

2.1 AGNES technique

AGNES [31;32] is based on two conceptual stages: i) an accumulation stage along which a suitable deposition program reduces the metal ion M^{2+} from the solution to Mº until a special situation of Nernstian equilibrium without concentration gradients of either M^{2+} or Mº is achieved. The gain, *Y*, in purged solutions is the ratio between the reduced metal concentration inside the amalgam $[M^0]$ and the free metal ion concentration $[M^{2+}]$ (being this $[M^{2+}]$ the same at the surface as in the bulk due to the absence of gradients in

the concentration profiles). The gain in purged solutions, for the eventual equilibrium potential E_1, can be computed from the peak potential (E_{peak}) of a Differential Pulse Polarogram (DPP)

$$Y = \frac{[M^0]}{[M^{2+}]} = \sqrt{\frac{D_M}{D_{M^0}}} \exp\left[-\frac{2F}{RT}\left(E_1 - E_{peak} - \frac{\Delta E}{2} \right) \right] \quad (3)$$

where D_M (7.03×10^{-10} m^2s^{-1} for Zn and 7.30×10^{-10} m^2s^{-1} for Cd) is the diffusion coefficient for the free metal ion in solution, D_{M^0} (1.81×10^{-9} m^2s^{-1} for Zn and 1.60×10^{-9} m^2s^{-1} for Cd) is the diffusion coefficient for the reduced metal inside the amalgam, F is the Faraday constant, R is the gas constant, T is the temperature and ΔE is the pulse amplitude.

Once equilibrium is reached, the solution is left during a certain time (waiting stage for t_w, usually, 50 s) in quiescent conditions with the same E_1. We call I_{Ox} to the measured current (without stirring) at the end of the first stage (see Figure SI-1, in the supporting information) which arises, mainly, from oxidants present in the solution such as O_2.

ii) the goal of the second stage is to quantify the accumulated metal M^0 inside the mercury amalgam. The response function can be the stripping faradaic current at a fixed time (e.g. 0.2 s for Hanging Mercury Drop Electrode (HMDE) [31]) or the stripped total faradaic charge Q accumulated during the deposition step [21;33]. Stripping chronopotentiometry (SCP) is very suitable for the quantification of Q, since blanks can be spared and metal interferences are easily avoided [22;34]. In SCP, the analytical signal is the time taken for reoxidation (transition time τ) [35] while applying a constant oxidizing current I_s (e.g. I_s=10^{-9} A for HMDE or 10^{-5} A for SPE) [22].

The I_s current can be seen as the combination of different components [22]: the faradaic current ($I_{faradaic} > 0$, the one important for AGNES purposes because it is associated to

the faradaic charge), the oxidants current ($I_{Ox} < 0$) and the capacitive current ($I_{capacitive} > 0$),

$$I_S = I_{faradaic} + I_{Ox} + I_{capacitive} \quad (4)$$

SCP can also be performed with a "chemical stripping" [36] (no I_s imposed, the oxidizing agent, e.g. oxygen, is present in the solution), as in this work. Since the analytical signal (τ) is measured above the baseline in a dt/dE vs E plot, the $I_{capacitive}$ is automatically subtracted and the accumulated charge can be computed as

$$Q = -I_{Ox}\tau \quad (5)$$

Faraday's law and eqn. (3) lead to the proportionality between the faradaic charge and the free metal concentration, which in purged systems reads:

$$Q = nFV_{Hg}[M^0] = \eta_Q Y[M^{2+}]^* \quad (6)$$

where η_Q is a proportionality factor that can be experimentally determined by performing a calibration.

2.2 Reagents and equipments

Zn and Cd 1000 ppm stock solutions were obtained from Merck. The total ionic strength was 0.01 M with supporting electrolyte KNO_3 purchased from Fluka (Trace Select). Nitrilotriacetic acid (NTA) and glycine were used as ligands (Fluka, ReagentPlus, ≥99%). Nitric acid (69-70%, Fluka Analytical for trace metal analysis), potassium hydroxide (0.1 M or 1 M, Fluka Analytical) and mercury(II) nitrate (atomic adsorption standard) was obtained from Merck. The pH-buffers MOPS (3-(N-morpholino)-propanesulfonic acid) and MES (2-(N-morpholino)-ethanesulfonic acid) were purchased from Sigma-Aldrich. Synthetic river water was used to perform measurements at pH* around 7.0 due to its buffer capacity. It was prepared with 0.01 M

$NaHCO_3$ (obtained from Merck, ≥99%), 2×10^{-3} M $CaCl_2$ (Scharlau, ≥99%), 10^{-3} $MgSO_4$ (Probus, ≥99%) and 5×10^{-4} M KNO_3.

Working solutions were diluted by ultrapure water (Milli-Q plus 185 System, Millipore) of 18 MΩ cm. In some experiments, purified water-saturated nitrogen N_2 (99.999%) was used for the purging of solutions.

Screen Printed Electrodes were prepared following previously published procedures [13;37] with polystyrene support for serigraphy (Sericol), mesitylen (Aldrich) and commercial ink (Acheson Colloids).

Voltammetric measurements were carried out using an Eco Chemie Autolab PGSTAT 12 potentiostat attached to a Metrohm 663 VA Stand and to a computer by means of the GPES 4.9 (Eco Chemie) software package. DPP parameters used in this work have been: modulation time 10 ms, interval time 1 s, step potential 0.00105 V and modulation amplitude 0.04995 V. DPPs were performed with a Metrohm multimode mercury drop electrode with the largest drop in our stand (drop 3) which corresponds to a radius of r_0=4.23×10^{-4} m. The auxiliary electrode was a glassy carbon electrode and the reference electrode was: i) Ag | AgCl | KCl (3 mol L^{-1}) encased in a 1 or 0.1 mol L^{-1} KNO_3 jacket (ref. 6.0726.100 from Metrohm). A glass combined electrode (Orion 9103) was attached to an Orion Research 720A ionanalyzer and introduced sporadically in the cell to control the bulk pH (pH^*). A glass jacketed cell provided by Metrohm, thermostated at 25.0ºC, was used in all the measurements.

3. Reaction-diffusion model for the steady-state pH profile in non-purged solutions

3.1 Experimental evidence for pH variation

The standard application of AGNES in solutions without deaerating led to unexpected results. Indeed, deposition potentials (corresponding to typical gains computed with DPP expression (3)) were applied with stirring for typical times (t_1) to samples

containing Zn^{2+} or Cd^{2+} ($c_{T,M}$ from 2.5×10^{-7} to 1.5×10^{-6} M) and pH between 4.0 and 7.5. The applied gains have been between Y=500 to 5000 (E_1 from -1.059 to -1.088 V for Zn^{2+} or E_1 from -0.637 to -0.667 V for Cd^{2+}), with t_1 between 350 and 1050 s and t_w=50 s. However, no signal could be measured in the non-purged solutions.

It was necessary to apply much more negative deposition potentials (for instance, E_1=-1.160 V for Zn^{2+} and E_1=-0.710 V for Cd^{2+}), which correspond to huge gains, $Y=1.3\times10^6$ for Zn^{2+} and $Y=1.1\times10^6$ for Cd^{2+} according to eqn. (3), to measure a signal (i.e. accumulated charge) around the same order to the one measured in a classical purged AGNES experiment at Y=500 and 5000, respectively [22]. Surprisingly, the deposition times needed to reach constant analytical signal were also t_1 from 350 to 1050 s and t_w=50 s, much shorter than the expected ones for the large Y supposedly prescribed.

An increase of the surface pH (pH^S), due to the reduction of oxygen and the consumption of protons (eqn. (1) and (2)) and the generation of hydroxide ions, can justify the previous observations. Because the analytical response is recorded after sufficiently long deposition times, once I_{Ox} has reached a stable value, all concentration profiles in the solution side are in steady state. Under these conditions, the local pH close to the electrode surface is higher than the bulk pH due to the oxygen reduction, and Zn(II) is transported towards the electrode as free Zn at the same rate as hydroxides and complexes of Zn (together) move back towards the bulk (see in Figure 1 a schematic representation of the expected steady-state concentration profiles in a non-purged sample). We call $[M^{2+}]^S$ to the metal concentration at the mercury surface and $[M^{2+}]^*$ to the bulk metal concentration (Figure 1). The fact that these two metal ion concentrations are different by the end of the deposition stage results in the observed anomalies and breaks the first principle of AGNES (absence of gradients in the

concentrations profiles). One could call SSNES (Steady State Nernstian Equilibrium Stripping) to the resulting technique, but, in this work, we prefer to keep the term AGNES even if it is clear that, by the end of the first stage, there is a steady-state non-uniform concentration profile of the free metal ion when the oxygen interference appears.

3.2 The I_{Ox} current

The I_{Ox} behaviour during the waiting stage has been examined along different t_w in non-purged solutions, with either Zn^{2+} or Cd^{2+}. AGNES has been performed in a synthetic river solution with $c_{T,Zn}$=0.53 μM, pH=7.5 and E_1=-1.160 V (t_1-t_w=500 s) or with $c_{T,Cd}$=0.25 μM, pH=6.5 and E_1=-0.685 V (t_1-t_w=1000s). The oxidants current takes, at least, t_w =150 s to stabilize for both Zn^{2+} and Cd^{2+} (Figure SI-1). We suggest using waiting times t_w not shorter than 150 s in order to work with a stabilized value of I_{Ox} which is key for the quantification step (see eqn. (5)).

In replicate experiments, I_{Ox} current might take around 2 hours to cease a slow drift (probably due to oxygen equilibration at the temperature of the experiment), and does not depend on the metal concentration or pH*. For instance, the measured I_{Ox} value does not change significantly in a non-purged synthetic river water with $c_{T,Zn}$=1.5 μM and pH* between 3.5 and 9.1 (I_{Ox} =5.0 ±0.1 μA).

The found I_{Ox} current in non-purged solutions for Zn^{2+} was around 4.0±1.0 μA whereas for Cd^{2+} was 2.8±0.6 μA. For comparison, I_{Ox} in a purged sample is around 50-300 nA.

3.3 Model

3.3.1 Assumptions and formulation of the model

Given the much higher concentration of dissolved oxygen (around 2.67×10^{-4} M, [38]) than that of the analyte metals (below micromolar), we start with the bold assumption that pH^S is essentially determined by the level of bulk dissolved oxygen and not by the fluxes involving species with M(II). The value of $[M^{2+}]^S$ is just, then, the one adapting to the local pH, analogously as an acid-base indicator (in small amount) adapts to the pH of the solution.

Because of the observation of lack of impact of pH on I_{Ox}, we also assume that the limiting step in the reduction of O_2 is its arrival, by just diffusion, to the electrode surface [39;40]. If a mole of O_2 accepts n_e moles of electrons (by a combination of reactions (1) and (2) [2]), a charge n_eF is injected to the working electrode surface. In steady state and assuming just diffusion (no migration), this charge is transported from the electrode surface towards the bulk solution by negatively charged species (OH^- and B^-, the anion of the buffer HB) or from the bulk solution towards the electrode surface by positively charged ones, so that, at any spatial position [41]:

$$n_e J_{O_2} = J_{OH^-} - J_{H^+} + J_{B^-} \tag{7}$$

where we take the convention of positive fluxes for those species in solution moving towards the electrode surface. Notice that the relative weight of the individual fluxes of the r.h.s. of eqn. (7) can change with the spatial position.

The steady-state continuity eqns. for the considered species are:

$$0 = \frac{\partial[OH^-]}{\partial t} = D_{OH^-}\frac{\partial^2[OH^-]}{\partial x^2} - k_{a,w}[H^+][OH^-] + k_{d,w} \tag{8}$$

$$0 = \frac{\partial[H^+]}{\partial t} = D_{H^+}\frac{\partial^2[H^+]}{\partial x^2} - k_{a,w}[H^+][OH^-] + k_{d,w} - k_{a,B}[H^+][B^-] + k_{d,B}[HB] \tag{9}$$

$$0 = \frac{\partial[B^-]}{\partial t} = D_{B^-}\frac{\partial^2[B^-]}{\partial x^2} - k_{a,B}[H^+][B^-] + k_{d,B}[HB] \tag{10}$$

$$0 = \frac{\partial[\mathrm{HB}]}{\partial t} = D_{\mathrm{HB}} \frac{\partial^2[\mathrm{HB}]}{\partial x^2} + k_{\mathrm{a,B}}\left[\mathrm{H^+}\right]\left[\mathrm{B^-}\right] - k_{\mathrm{d,B}}[\mathrm{HB}] \quad (11)$$

where D_j is the diffusion coefficient of species j and $k_{\mathrm{a},j}$ and $k_{\mathrm{d},j}$ are, respectively, the association and dissociation rate constants. In order to cancel the kinetic terms, we add eqn. (8) to (10) and subtract eqn. (9):

$$0 = \frac{\partial\left(\left[\mathrm{OH^-}\right] - \left[\mathrm{H^+}\right] + \left[\mathrm{B^-}\right]\right)}{\partial t} = D_{\mathrm{OH^-}} \frac{\partial^2\left[\mathrm{OH^-}\right]}{\partial x^2} - D_{\mathrm{H^+}} \frac{\partial^2\left[\mathrm{H^+}\right]}{\partial x^2} + D_{\mathrm{B^-}} \frac{\partial^2\left[\mathrm{B^-}\right]}{\partial x^2} = \frac{\partial^2 \Omega(x)}{\partial x^2} \quad (12)$$

where

$$\Omega(x) = D_{\mathrm{OH^-}}\left[\mathrm{OH^-}\right] - D_{\mathrm{H^+}}\left[\mathrm{H^+}\right] + D_{\mathrm{B^-}}\left[\mathrm{B^-}\right] \quad (13)$$

The solution of eqn. (12) with boundary conditions corresponding to the fixed surface (x=0) and bulk (x=δ) concentrations is:

$$\Omega(x) = \Omega^{\mathrm{S}} + \left(\Omega^{*} - \Omega^{\mathrm{S}}\right)\frac{x}{\delta} \quad (14)$$

We recognize

$$\frac{d\Omega}{dx} = J_{\mathrm{OH^-}} - J_{\mathrm{H^+}} + J_{\mathrm{B^-}} \quad (15)$$

so that the balance of fluxes (7) can now be written as:

$$n_{\mathrm{e}} \frac{D_{\mathrm{O_2}}\left[\mathrm{O_2}\right]^{*}}{\delta} = \frac{\Omega^{*} - \Omega^{\mathrm{S}}}{\delta} \quad (16)$$

where we have taken the same diffusion layer thickness (δ) for the diffusion of O_2 (which is independent) and those of the other species (which are coupled via the interconversion processes). This constitutes a third key assumption, because it leads to the surprising consequence that pH^S should be independent of the thickness of the diffusion layer and differentiates our present model from that of Auinger *et al.* [41]. These authors studied the pH profiles produced by a Pt rotating disk electrode in solutions with dissolved H_2 (and negligible O_2) with basically the same assumptions as

in the present model (where hydrogen evolution is considered negligible due to the overpotential on the mercury electrode).

For simplicity, we take an identical diffusion coefficient for the protonated and deprotonated form of the buffer. Summation of eqn. (10) and (11) with the appropriate boundary conditions leads to [41-43]:

$$\left[\mathrm{B}^{-}\right]+\left[\mathrm{HB}\right]=\left[\mathrm{B}^{-}\right]^{*}+\left[\mathrm{HB}\right]^{*} \tag{17}$$

A fourth assumption is that all homogeneous reactions are at equilibrium (i.e. full lability). We consider that the background electrolyte provides a constant ionic strength, so that the activity coefficients do not change and we can work with conditional equilibrium constants (without any specific notation). Activity coefficients in this work have been computed with Davies expression. Thus, eqn. (16) can be written just in terms of one unknown: the concentration of OH at the surface, $[OH^-]^S$

$$\begin{aligned} n_{\mathrm{e}} D_{\mathrm{O_2}} \left[\mathrm{O_2}\right]^{*} = {} & D_{\mathrm{OH^-}} \left(\left[\mathrm{OH^-}\right]^{*} - \left[\mathrm{OH^-}\right]^{\mathrm{S}}\right) - D_{\mathrm{H^+}} \left(\frac{K_{\mathrm{w}}}{\left[\mathrm{OH^-}\right]^{*}} - \frac{K_{\mathrm{w}}}{\left[\mathrm{OH^-}\right]^{\mathrm{S}}}\right) + \\ & + D_{\mathrm{B}} \left(\left[\mathrm{B}^{-}\right]^{*} + \left[\mathrm{HB}\right]^{*}\right) \left(\frac{\left[\mathrm{OH^-}\right]^{*}}{\left[\mathrm{OH^-}\right]^{*} + K_{\mathrm{HB}} K_{\mathrm{w}}} - \frac{\left[\mathrm{OH^-}\right]^{\mathrm{S}}}{\left[\mathrm{OH^-}\right]^{\mathrm{S}} + K_{\mathrm{HB}} K_{\mathrm{w}}}\right) \end{aligned} \tag{18}$$

where K_{w} is the conditional water product and K_{HB} is the conditional association equilibrium constant. Physically, Eqn. (18) –which is analogous to eqn. (22) in [41]- indicates that the contributions to the charge flux splits in terms as if the diffusion processes of the various species from the bulk (with a common δ) towards the electrode surface were totally independent, while, in fact, they are strongly coupled [44;45] (see section 3.3.3 on profiles, below).

Eqn. (18) is a cubic equation which can be easily solved with standard procedures [46]. Once $[OH^-]^S$ is found, the computation of pH^S is straightforward. So, this simple model predicts that pH^S depends on:

i) the number of exchanged electrons, which is a function of the deposition potential and has been estimated from the ratio of oxidants currents given that

$$I_{Ox} = n_e \frac{D_{O_2}[O_2]^*}{\delta} \quad (19)$$

Figure 2 shows measured I_{Ox} for various deposition potentials (E_1 between -0.60 and -1.30 V). The I_{Ox} decreases (in absolute value) as the deposition potential becomes more positive which correlates with a change in the number of electrons transferred as we move from the pathway showed in reaction (1) to reaction (2). We have considered that 2 electrons are transferred when applying E_1 corresponding to Cd (E_1 from -0.600 to -0.750 V, I_{Ox}≈-3.44 μA). For Zn (E_1 between -1.050 and -1.160 V, I_{Ox} from -4.38 to -5.30 μA), the number of electrons exchanged have been estimated between 2.5 and 3.1 (Figure 2), from the relationship between the reference Cd I_{Ox}-value and Zn I_{Ox}-value;

ii) the level of dissolved oxygen;

iii) the bulk pH^*

and iv) the buffer properties of the medium (total concentration, diffusion coefficient and association equilibrium constant),

but pH^S does not depend on the size characteristics, such as the diffusion layer thickness (i.e. level of stirring) or the surface area. Notice that no adjustable parameter is required for this model.

3.3.2 The particular case without buffer

In a system without buffer, the last term in Eqn. (18) disappears and, then, the resulting quadratic eqn. leads to the explicit expression (similar to eqn. 17 in ref. [41])

$$\left[\mathrm{OH^-}\right]^{\mathrm{S}} = \frac{1}{2}\left(\frac{n_{\mathrm{e}} D_{\mathrm{O_2}} \left[\mathrm{O_2}\right]^*}{D_{\mathrm{OH^-}}} + \left[\mathrm{OH^-}\right]^* - \frac{D_{\mathrm{H^+}} K_{\mathrm{w}}}{D_{\mathrm{OH^-}} \left[\mathrm{OH^-}\right]^*}\right) + \sqrt{\left(\frac{n_{\mathrm{e}} D_{\mathrm{O_2}} \left[\mathrm{O_2}\right]^*}{2 D_{\mathrm{OH^-}}} + \frac{\left[\mathrm{OH^-}\right]^*}{2} - \frac{D_{\mathrm{H^+}} K_{\mathrm{w}}}{2 D_{\mathrm{OH^-}} \left[\mathrm{OH^-}\right]^*}\right)^2 + \frac{D_{\mathrm{H^+}} K_{\mathrm{w}}}{D_{\mathrm{OH^-}}}} \tag{20}$$

A detailed analysis of this simple expression leads to predict a practically constant

$$\mathrm{pH^S} \approx 14 + \log\left(\gamma_1 \frac{n_{\mathrm{e}} D_{\mathrm{O_2}} \left[\mathrm{O_2}\right]^*}{D_{\mathrm{OH^-}}}\right) \tag{21}$$

which is around 10.3 for the typical values (see Table SI-1) and n_e=2. This value is reached whenever

$$\mathrm{pH^*} > 14 + \log\left(\gamma_1 \frac{n_{\mathrm{e}} D_{\mathrm{O_2}} \left[\mathrm{O_2}\right]^*}{D_{\mathrm{H^+}} K_{\mathrm{w}}}\right) \approx 3.7 \tag{22}$$

while $\mathrm{pH^S} \approx \mathrm{pH^*}$ below this critical value or above pH*>10.8 (see continuous blue line in Figure 3).

3.3.3 Model concentration profiles

Once $[\mathrm{OH^-}]^{\mathrm{S}}$ is known from either (18) or (20), all profiles can be easily computed, provided that a thickness of the diffusion layer is assumed. For instance, in the general case with buffer, the slope $\left(\Omega^* - \Omega^{\mathrm{S}}\right)/\delta$ in eqn. (14) can be computed with eqn. (16) and the intercept Ω^{S} is found by replacing the surface concentrations (which are in equilibrium) at the electrode surface:

$$\Omega^{\mathrm{S}} = D_{\mathrm{OH^-}} \left[\mathrm{OH^-}\right]^{\mathrm{S}} - D_{\mathrm{H^+}} \frac{K_{\mathrm{w}}}{\left[\mathrm{OH^-}\right]^{\mathrm{S}}} + D_{\mathrm{B}} \left(\left[\mathrm{B^-}\right]^* + \left[\mathrm{HB}\right]^*\right) \frac{\left[\mathrm{OH^-}\right]^{\mathrm{S}}}{\left[\mathrm{OH^-}\right]^{\mathrm{S}} + K_{\mathrm{HB}} K_{\mathrm{w}}} \tag{23}$$

For a given x, eqn. (14) yields an eqn. for $[\mathrm{OH^-}]$ at that position:

$$D_{OH^-}\left[OH^-\right]-D_{H^+}\frac{K_w}{\left[OH^-\right]}+D_B\left(\left[B^-\right]^*+\left[HB\right]^*\right)\frac{\left[OH^-\right]}{\left[OH^-\right]+K_{HB}K_w}=\Omega^S+\left(\Omega^*-\Omega^S\right)\frac{x}{\delta} \quad (24)$$

Once $[OH^-]$ at a certain x is known, all other concentrations follow from the equilibrium relationships such as:

$$\left[H^+\right]=\frac{K_w}{\left[OH^-\right]} \quad (25)$$

or

$$\left[B^-\right]=\left(\left[B^-\right]^*+\left[HB\right]^*\right)\frac{\left[OH^-\right]}{\left[OH^-\right]+K_{HB}K_w} \quad (26)$$

The concentration profiles seen in Figure 4 show that the charge can be mainly carried by different species at different distances from the surface electrode: OH^- up to ca. $\delta/6$, HB and B^- from ca. $\delta/6$ to ca. $\delta/2$ and H^+ for $x > \delta/2$. The formal species Ω increases linearly from the electrode surface up to $x=\delta$, but the individual species follow a very different pattern which is far away from the naïve linear idea suggested by the global flux (see eqn. (18)) being the summation of terms corresponding to the differences between each species at the $x=\delta$ and at the electrode surface.

.

4. Relationship between accumulation and applied potential

4.1 Influence of deposition potential, time and stirring on AGNES response under non-purged conditions

The model expound in section 3 derives pH^S from the level of oxygen and buffering capacity, with assumed negligible impact of the existing trace metal. We consider that the concentration of free metal then adapts to the existing pH at each spatial position. Due to the gradient of $[M^{2+}]$ along the solution, a unique definition of the gain, Y in eq.

(3), no longer holds. Assuming that Nernstian Equilibrium is eventually reached, we define the surface gain Y^S (Figure 1), as

$$Y^S = \frac{[M^0]}{[M^{2+}]^S} = \sqrt{\frac{D_M}{D_{M^0}}} \exp\left[-\frac{nF}{RT}\left(E_1 - E_{peak} - \frac{\Delta E}{2}\right)\right] \quad (27)$$

On the other hand, we can also define a bulk gain Y^*, as the ratio between reduced metal and free bulk concentrations which can be computed from Faraday's law

$$Y^* \equiv \frac{[M^0]}{[M^{2+}]^*} = \frac{Q}{nFV_{Hg}[M^{2+}]^*} \quad (28)$$

where Q is the experimental accumulated charge, V_{Hg} is the electrode mercury volume (usually, 1.9×10^{-6} m^3) and $[M^{2+}]^*$ is the bulk free analyte concentration (which can be estimated with Visual Minteq in a synthetic solution or measured with other methods such as AGNES with purging, if possible). As seen in Figure 1, $Y^* << Y^S$.

For instance, in a non-deaerated sample containing $c_{T,Zn}$=1.5 µM with pH*=4.9, a classical 1-Pulse AGNES program [31;32] has been applied (E_1=-1.160 V, $Y^S=1.3\times10^6$), with stirring, and no further change of the analytical response appears for t_1 longer than 650 s and t_w=150s, indicating the attainment of the steady state. At the end of the experiment, the computed Y^* is just 500 (about the same order as the gains usually applied in a purged solution), which is in agreement with the deposition times needed.

However, if we try to apply even higher Y^S (i.e. E_1>-1.170 V), the application of AGNES in non-purged samples with a 1-Pulse program could be problematic, due to the longer deposition times required and the involved risk of not really achieving the steady state (if we are misled by too small increases of the signal with increasing times). Figure 5 (blue square markers) shows the retrieved charges in some AGNES experiments performed in a $c_{T,Zn}$=0.76 µM (pH*=4.4) at different Y^S, from E_1=-1.150 V to -1.190 V, with deposition times t_1 from 300 to 1650s and t_w=150s. Erroneously, a steady state seemed to be reached in all experiments, since the aforementioned t_1 were tested for

every Y^S analyzed and, in all cases, the measured accumulated charges appeared to be practically constant for sufficiently long times (up to 1500 s). One of the properties of AGNES is the linear proportionality between the analytical signal and the imposed gain: if Y doubles, so does the analytical signal. The continuous line in Figure 5 represents the expected accumulated charges if a steady state had been reached for all the imposed Y^S and it is clear that the experimental measured 1-Pulse charges (blue square markers, Figure 5) for $Y^S > 5.0\times10^6$ did not reach it. We believe that the deposition times range used for the highest gains applied were too short to reach steady state with the prescribed pre-concentration. Very similar results were obtained for Cd^{2+} (data not shown).

In order to reduce the deposition time, the first stage can be split into two sub-stages in a variant called 2-Pulses [26]: a potential step that corresponds to diffusion limited conditions with stirring (for instance, $E_{1,a}$=-1.300 V, $t_{1,a}$) followed by a potential step (E_1) at the desired concentration gain. Due to the need of stabilized steady-state profiles (which change when switching the stirring on and off), we have taken just an unstirred second sub-stage (i.e. $t_{1,b}$=0 in the notation of [26], see scheme in Figure SI-2), which implies working with longer t_w (i.e. application of E_1 without stirring longer than the usual 50 s) that also helps in reaching steady I_{Ox} currents. An example of the optimisation of the deposition times $t_{1,a}$ and t_w is shown in Figure SI-3.

A linear relationship between Q and Y^S is obtained for sufficiently long deposition programs (see red circles in Figure 5 for optimized 2-Pulses programs), even for very large Y^s.

The theoretical model described in Section 3.3 implies a lack of influence from the thickness of the diffusion layer on the local pH^S and the corresponding modification of the speciation in the surroundings of the electrode (i.e $[M^{2+}]^S$ is independent of stirring).

To check this fact, we run a 1-Pulse AGNES measurement (E_1=-1.160 V and t_1 between 400 and 8150 s and t_w=150 s) where the deposition stage was carried out with and without stirring in a solution with $c_{T,Zn}$=1.25 μM at pH*=4.35. The waiting stage in both experiments was sufficiently long (t_w at least 150 s) to stabilize properly the concentration profiles in the solution. The stirred experiment took 500 s to reach steady state (see blue asterisk markers in Figure 6), whereas the unstirred one needed around 5000 s to achieve it (red circle markers in). Both series of experiments achieved the same accumulated charge, which was expected from the lack of influence from the thickness of the diffusion layer. However, it might also happen that the waiting period t_w=150 s was long enough to restore the surface concentrations and accumulated Mº to the same values as the procedure without any stirring, but this would also mean that the separation between stirred and unstirred situations is not large. Results in Figure 6 are also consistent with previously data observed in purged solutions where the stirred deposition procedures can be 10 times shorter than the unstirred ones to reach equilibrium.

4.2 Effect of the SPE resistance

Screen Printed Electrodes (Section 2.2) exhibit a resistance (R) around 2.3±0.2 kΩ between the electrical contact and the working electrode surface. This large resistance directly affects on the deposition potential applied during an AGNES measurement, especially in non-purged solutions where the measured currents are particularly high (I_{Ox}≈4.0 μA). According to Ohm's law, the nominal deposition potential $E_1^{nominal}$ (the one we impose between the reference and the working electrode from the potentiostat) is influenced by the system resistance and the measured current I_{Ox}. Due to the high I_{Ox}

value in a non-purged experiment, the product $I_{Ox}R$ (11±1 mV) cannot be neglected and has to be taken into account to estimate the real applied deposition potential E_1^{real},

$$E_1^{nominal} = I_{Ox}R + E_1^{real} \quad (29)$$

The product $I_{Ox}R$ can be more accurately determined from AGNES experiments. Thus, we have compared the retrieved charges when the steady state has been reached in a purged and a non-purged solution containing $c_{T,Zn}$=1.5 μM at pH*=2.5 (this acidic medium allows to simplify the non-purged system by eliminating the appearance of a local pH different from the bulk one). In both cases, we have applied $E_1^{nominal}$=-1.055 V (t_1=650 s and t_w=150 s). At the end of the experiment, the accumulated charge in the purged solution is 2.5 times higher than the non purged one. By combining eqns. (6), (3) and (29), the expected relationship between both purged (Q^{purged}) and non-purged ($Q^{non\text{-}purged}$) charges is,

$$\frac{Q^{purged}}{Q^{non\text{-}purged}} = \exp\left[-\frac{nF}{RT}(I_{Ox}^{purged} - I_{Ox}^{non\text{-}purged})R\right] \quad (30)$$

where I_{Ox}^{purged} and $I_{Ox}^{non\text{-}purged}$ correspond, respectively, to the oxidants current measured in a purged and non-purged sample.

Using eqn. (30) and the retrieved experimental charges, we have obtained that $(I_{Ox}^{purged} - I_{Ox}^{non\text{-}purged})R$ equals to, approximately, -12.0 mV. These mV corresponds to the experimental difference between the nominal and the real deposition potential applied, eqn. (29), and are in agreement with the previously estimated value (11±1 mV). Those -12.0 mV have been taken into account to re-compute the real imposed Y^S gains.

In purged samples, the measured I_{Ox} (with SPE) exhibits values around 50-300 nA, very low compared with the non-purged ones. In this case, we can consider negligible the difference between the $E_1^{nominal}$ and E_1^{real} ($I_{Ox}R$ < 1mV).

When performing the measuring of a sample, the difference between the nominal and the applied potentials is not a problem, since it cancels out between the calibration and the measurement, provided a same level of oxygen.

5. AGNES as a tool to measure the metal ion surface concentration and estimate pH in a non-purged sample

AGNES can directly provide the surface metal concentration by combining eqns. (27) and Faraday's law (parallel to eqn. (6) or eqn. 1 in [47]):

$$[\mathrm{M}^{2+}]^{\mathrm{S}} = \frac{Q}{\eta_{\mathrm{Q}} Y^{\mathrm{S}}} \tag{31}$$

and, then, estimate the corresponding change of pH^{S} in solutions without removal of oxygen. This procedure seems simpler than other voltammetric methods that estimated the surface concentration of the oxidized metal during the stripping stage.

Let g be the quotient between the surface gain Y^{S} (27) and the bulk gain Y^*, eqn. (28), which is also the ratio between the bulk concentration of the metal, $[\mathrm{M}^{2+}]^*$, and the surface one, $[\mathrm{M}^{2+}]^{\mathrm{S}}$

$$g \equiv \frac{Y^{\mathrm{S}}}{Y^*} = \frac{[\mathrm{M}^{2+}]^*}{[\mathrm{M}^{2+}]^{\mathrm{S}}} \tag{32}$$

Simple algebra leads to an extension of eqn. (6) to cases where $\mathrm{pH}^{\mathrm{S}} \neq \mathrm{pH}^*$ hinders the attainment of the absence of gradients in the concentration profiles:

$$Q = \frac{\eta_{\mathrm{Q}} Y^{\mathrm{S}} [\mathrm{M}^{2+}]^*}{g} \tag{33}$$

g, thus, quantifies the interference of the dissolved oxygen due to the change in the speciation close to the working electrode. When g is 1, it means that $Y^{\mathrm{s}} = Y^*$ and, therefore, no increase in the local pH is expected (we are in a purged-like situation, under absence of gradients). As g increases, higher pH-gradients lead to large changes

of the speciation in the vicinity of the electrode, which corresponds to a more relevant oxygen interference.

The theoretically expected *g* can be easily computed from the model, if we further assume that all complexes of Zn are fully labile and with the same diffusion coefficient. This hypothesis leads to a homogeneous steady-state total Zn concentration at any spatial position [42;43]:

$$c_{\mathrm{T,Zn}}^{\mathrm{S}} = c_{\mathrm{T,Zn}}^{*} \tag{34}$$

so,

$$[\mathrm{M}^{2+}]^{\mathrm{S}}\left\{1+\sum\beta_i^{\mathrm{OH}}\left([\mathrm{OH}^-]^{\mathrm{S}}\right)^i+\sum K_j[{}^j\mathrm{L}]^{\mathrm{S}}\right\}=\left[\mathrm{M}^{2+}\right]^{*}\left\{1+\sum\beta_i^{\mathrm{OH}}\left([\mathrm{OH}^-]^{*}\right)^i+\sum K_j[{}^j\mathrm{L}]^{*}\right\} \tag{35}$$

where β_i^{OH} is the cumulative constant for the hydroxocomplex with *i* OH-groups, ${}^j\mathrm{L}$ refers to a ligand with index *j* and K_j is its complexation constant with Zn. Solving for the quotient of free concentrations:

$$g=\frac{[\mathrm{M}^{2+}]^{*}}{[\mathrm{M}^{2+}]^{\mathrm{S}}}=\frac{1+\sum\beta_i^{\mathrm{OH}}\left([\mathrm{OH}^-]^{\mathrm{S}}\right)^i+\sum K_j[{}^j\mathrm{L}]^{\mathrm{S}}}{1+\sum\beta_i^{\mathrm{OH}}\left([\mathrm{OH}^-]^{*}\right)^i+\sum K_j[{}^j\mathrm{L}]^{*}} \tag{36}$$

The value of the theoretical *g* for Cd and Zn exhibits a kind of “step” shape when plotted against pH* for different number of electrons exchanged (see Figure 7). However, small changes in the oxygen level, composition of the sample, number of transferred electrons, etc. impact on pH^{S}. For instance, Figure 8 shows the significant variation of the *g* factor for small changes in pH^{S} in the range 10-11, for a $c_{\mathrm{T,Cd}}$=0.3 μM solution with increasing amounts of NTA from 0 to 0.26 μM. This fact leads to a relatively large variation in the “plateau” value of Fig 7. High total concentrations of Cd and high pH values can lead to the formation of insoluble metal hydroxides rendering AGNES measurements not possible.

A second limitation of eqn. (36) is that this expression cannot be used in systems of unknown composition (e.g. in a river water with organic matter), although it can provide some guidelines when the speciation is mostly ruled by OH^- complexation.

More pragmatically, g can be computed in solutions where $[M^{2+}]^*$ is known experimentally by using eqn. gInterference(33) and the constant η_Q which can be obtained from a calibration plot in a purged sample or from the volume of Hg ($\eta_Q = nFV_{Hg}$). Once g and $[M^{2+}]^*$ are known, the surface concentration $[M^{2+}]^S$ can be obtained using the definition of g (32).

Either directly with eqn. (31) or via g, $[M^{2+}]^S$ can be found, and its difference from $[M^{2+}]^*$ can be useful in the estimation of pH^S. Indeed, with a modeling software like Visual Minteq, we can estimate the corresponding surface pH^S by looking for the pH that (with the known composition of the bulk of the sample) yields as free metal concentration the just computed $[M^{2+}]^S$. This estimation can result in a wide range of pH^S (if, for this composition, the free metal concentration is practically insensitive to pH-changes) and does not take into account the changes in composition at the electrode surface other than those elicited by the pH change.

The surface metal concentration $[M^{2+}]^S$ and pH^S have been estimated experimentally with AGNES in different buffered or non-buffered samples without deaerating.

i) A non-buffered sample with $c_{T,Zn}$=1.5 μM at pH*=2.1 has been measured with E_1=-1.055 V (Y^S=900) when a steady state is reached (t_1=650-1150 s and t_w=150 s). The computed g factor has been approximately 1 (see Table SI-1) which means that the system reaches absence of concentration gradients ($Y^S \approx Y^*$) with no influence from the dissolved oxygen. This fact agrees with the applied deposition potential E_1 which was similar to the usual ones in purged solutions. Under these conditions, Visual Minteq estimates that the surface pH could be anywhere between 2.1 ($pH^* \approx pH^S$) and 8.2, since

no changes in the speciation are expected in this pH range (see leftmost ▲ marker in Figure 9 and Table SI-1). Previously published results, where Zn was measured with chronopotentiometry in a very acidic media, pointed to the same conclusions (pH^S between 2 and 4) [39].

The same solution has been examined at pH*=4.9, but a much more negative deposition potential was needed (E_1=-1.160 V, t_1=650-1150 s and t_w=150 s) to obtain a measurable signal. The oxygen interference becomes more relevant (g=2710) and the estimated pH^S is 10.2 (rigthmost ▲ in Figure 9 and Table SI-1). These results agree with previously estimated pH values using Anodic Stripping Techniques [8;48].

Also under non-buffered conditions, solutions containing $c_{T,Cd}$=1.0 or 1.5 µM have been examined at pH*=2.2, 4.1, 5.1 and 6.6 (fixed with the addition of KOH or HNO_3). AGNES 1-Pulse with E_1 -0.675 V (t_1=650-1150 s and t_w=150 s) has been applied to the samples with pH*=2.2, 4.1 and 5.1 whereas a 2-Pulses AGNES procedure ($E_{1,a}$=-1.300 V, $t_{1,a}$=75 s, E_1=-0.705 V and t_w=500 s) has been applied for the sample with pH*=6.6. For the most acidic solution, the estimated pH^S could be from 2.2 to 9.3, since speciation practically does not change in this range of pH. In the samples with pH* from 4.1 to 6.6, the surface pH^S has been found to be more basic, from 10.0 to 10.6 (see Table SI-1 and ▲ markers in Figure 3).

ii) Increasing the buffer capacity of the sample can lead to less steep pH-gradients as already explained in Section 3. A sample with $c_{T,Zn}$=1.5 µM, [NTA]=1.5 µM and buffered with [MES]=0.01 M has been measured using AGNES (E_1 between -1.080 and -1.100 V, t_1=650-1150 s and t_w=150 s) at different pH* (5.0, 5.5, 6.0 and 6.4). Compared with the non-buffered solution, the deposition potentials needed are less negative, which agrees with the expected decrease in the pH-gradient. As expected, the g factor decreases (Table SI-1) and the local pH^S has appeared to be less basic, between

5.8 and 7.6 (see ● markers in Figure 9). Other reports [8;10] also pointed out the lower influence of dissolved oxygen in buffered samples.

Different buffers and ligands have also been tested. A $c_{T,Zn}$=1.0 µM sample buffered with [MOPS]=0.01 M has been analyzed in presence of [glycine]= 200 µM at pH* =7.6. AGNES conditions have been E_1=-1.110 V and t_1=650 s and t_w=150 s. The surface pH^S has been estimated to be between 8.7 and 8.9 (■ marker in Figure 9 and Table SI-1).

Very similar results have been found when a $c_{T,Cd}$=2.5 µM solution with [NTA]=1.5 µM and [MES]=0.01 M has been studied at pH*=5.0, 6.0 and 6.6 (E_1=-0.675 V, t_1=650-1150 s, t_w=150 s). pH^S have been estimated to be less basic, between 5.7 and 9.5, depending on the experiment (see ● in Figure 3 and Table SI-1).

In all cases, the local pH^S–values measured by AGNES (see markers in Figure 3) are in good agreement with the theoretical ones estimated in Section 3.3 (see Δ, ○ and □ markers in Figure 9 or the continuous and discontinuous lines in Figure 3) and corroborates the validity of both the theoretical model and the AGNES procedure. This fact indicates that AGNES can be a useful experimental tool to estimate the change of the local speciation during the analysis of a non-purged sample.

6. Speciation experiments

The performance of AGNES to retrieve the bulk free metal concentration (i.e. its original purpose) in non-purged samples has been analyzed by carrying out speciation experiments in synthetic solutions.

The key point of these measurements is to perform both the calibration and the speciation study under conditions where the oxygen interference is very similar in both solutions. The *g* factor allows estimating this interference (see Section 5, eqn. (33)) in

synthetic samples and gives a clue on when the free concentration experiment could be successful.

The parameter *g* depends on:

a) The level of dissolved O_2, which essentially determines pH^S. For finding $[M^{2+}]^*$, the calibration and the speciation sample should have similar oxygen levels and similar local speciation changes due to the pH increase. Buffering the samples could help to moderate the shift in pH^S in both solutions. In this work, we have analyzed the impact of the addition of MOPS and MES to a non-purged sample.

b) The composition of the samples. Not only does *g* depend on the pH^S, but also on the presence of ligands in the solution. When determining the free metal concentration $[M^{2+}]^*$, we seek calibration and sample systems with compositions where the same pH^S yields the same change in $[M^{2+}]^S$. This is possible when the speciation is dominated by known ligands (while unknown ones have a much smaller impact). Certain amounts of (unknown) ligand in the sample, and depending on the values of their complexation and protonation constants, could lead to an important change on its composition and, thus, to the attainment of different *g* values between the calibration and speciation experiment. At the end, this would result in an incorrect determination of the free metal concentration.

c) The number of exchanged electrons which, as already explained in section 3.2, is a function of the applied deposition potential.

First of all, we have measured the free metal concentration in a non-deaerated system with $c_{T,Cd}$=0.3 μM and NTA=0.13 and 0.20 μM at a non-buffered pH*=6.0. AGNES settings have been a 1-Pulse procedure with $E_{1,a}$=-0.711 V, t_1=1250-1600 s and t_w=150 s. The system calibration has been performed under the same non-purged conditions with a pH* fixed at 6.0 without buffer. The retrieved experimental free concentrations

are compared with the Visual Minteq predicted concentrations (red circle markers in Figure 10): the error increases from 25 % for [NTA]=0.13 μM to 43 % for [NTA]=0.20 μM. For this unbuffered experiment, while the local pH is comparable between the calibration and sample (pH^S has been estimated to be 10.7±0.1), its impact on the local free metal concentration is very much dependent on the NTA concentration. This last fact can be checked in Figure 8, where $g=[Cd^{2+}]^{pH^*=6.0}/[Cd^{2+}]$ has been computed, using Visual Minteq, for a solution with $c_{T,Cd}$=0.3 μM and increasing amounts of NTA for different pH^S–values. Under the speciation experimental conditions used ($pH^S \approx 10.7\pm0.1$), different theoretical g values are expected for the calibration, [NTA]=0 μM, and the speciation experiment, [NTA]=0.13 and 0.20 μM (Figure 8). These g values are in agreement with the experimental ones obtained (see Table SI-2) and explain the large errors in the determination of the free Cd^{2+} concentration without buffer (red circle markers in Figure 10).

A very similar speciation experiment, containing $c_{T,Cd}$=1.0 μM and [NTA] between 0.19 μM and 0.62 μM, has been carried out, but in presence of [MES]=0.01 M with pH* fixed at 6.7. AGNES parameters have been: E_1=-0.675 V, t_1 between 650 and 1150 s and t_w=150 s. The measured free Cd concentrations with AGNES have appeared to be in good agreement with the estimated ones by Visual Minteq (blue square markers in Figure 10) with an error between 3 and 8%. Compared with the non-buffered speciation experiment, the improvement on these results is believed to come from the addition of MES to the system. Under these conditions, the surface pH is estimated to be less basic and the computed g factor appears to be lower (less interference from the dissolved oxygen) as well as more similar between calibration and speciation (see Table SI-2).

We have also tackled a system with $c_{T,Zn}$=1.0 μM, different glycine concentrations (from 200 μM to 750 μM) at pH*=7.6 buffered with MOPS 0.01 M. AGNES settings

have been E_1=-1.110 V, t_1=650-1150 s and t_w=150 s. Under these conditions, pH^S has been estimated to be 8.8±0.1 (Figure 9 and Table SI-2) and the composition of the calibration and speciation samples are expected to be very similar (see computed *g* values in Table SI-2). The measured free Zn concentration with AGNES (blue square markers in Figure SI-4) are comparable to the estimated ones computed using Visual Minteq (red circle markers in Figure SI-4), with an error between 4 and 13 %.

In conclusion, AGNES can properly measure the free metal concentration in non-purged systems provided calibration and sample have a similar speciation shift when the local pH changes. The use of a buffer decreases the pH^S which translates into more accurate speciation measurements.

7. Conclusions

The increase of pH at the electrode surface, due to the reduction of dissolved oxygen in steady-state regime, can be modelled with assumptions such as negligible effect of trace metals, a common diffusion layer and full equilibrium of the reacting species. The model predicts that pH^S depends on the level of dissolved oxygen and on the bulk pH. If there is no buffer in the solution, the explicit equation (20) can be used, while, for a buffered solution, the cubic eqn. (18) has to be solved. Predicted and estimated pH^S values (from AGNES measurements in the probed systems) agree quite well (see Figures 3 and 9). The impact on pH^S of the number of exchanged electrons at different deposition potentials for a given metal (Figure 2) is relatively mild, but with large consequences for speciation (Figure 8). The modelled concentration profiles (see Figure 4) indicate that different species are the main transporters of charge in different regions of the diffusion layer.

Due to the difference between pH^S and pH*, the requisite of "absence of gradients" in the concentration profiles for the standard application of AGNES does not hold in non-purged solutions. The critical point is that the surface concentration $[M^{2+}]^S$ is different from the bulk concentration $[M^{2+}]^*$. So, the surface gain Y^S (prescribed by the applied potential computed with Nernst equation, see eqn. (27)) is different from the bulk gain Y^*, eqn. (28) (see Figure 1). However, AGNES does retrieve $[M^{2+}]^S$ directly (see eqn. (31)) and, via speciation computations, estimates pH^S.

The interference of oxygen in AGNES determination of the bulk free concentration is clearly noticed in the need of deposition potentials more negative than usual. This interference can be quantified by a factor *g* (see eqns. (32) and (33)), but –up to date- *g* can only be found in solutions where the free bulk concentration is already known (e.g. by comparison with an AGNES experiment in the purged solution). A strategy to determine bulk free metal concentrations in non-purged solutions with AGNES consists in looking for a calibration solution (where the composition is known) as similar as possible to the sample: "Similarity" should be understood in the sense that the changes in speciation due to the specific pH shift are practically the same in both solutions and the *g* factor (implicit in the slope of the calibration) can be assumed to be the same. The application of this strategy to some systems (e.g. Figure 10) led to disagreements below 15%.

Another impact of dissolved oxygen is the increase of the oxidation current at the end of the deposition stage of AGNES (I_{Ox}). This produces an IR voltage (see eqn. (29)) that needs to be taken into account for rigorous computations of the real gains, though the cancellation of the gain offsets between calibration and measurement provides reliable free concentrations without this correction.

Acknowledgments

This work was financially supported by the Spanish Ministry of Education and Science (Projects CTQ2009-07831, CTM2009-14612 and CTM2012-39183), from the "Comissionat per a Universitats i Recerca del Departament d'Innovació, Universitats i Empresa de la Generalitat de Catalunya"

8. References

Figures

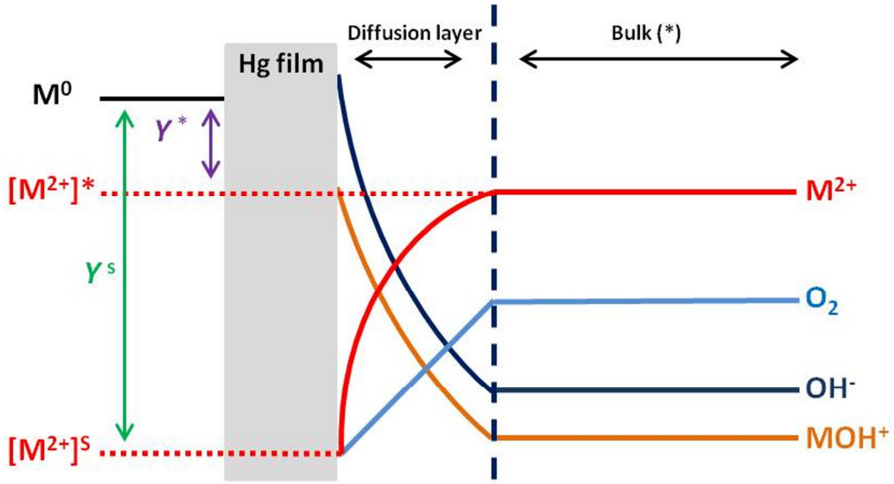

Figure 1. Schematic steady-state concentration profiles in a non-purged solution. Dissolved oxygen (blue line) produces OH^- ions at the electrode surface of the Hg film which diffuse back towards the bulk of the solution (dark blue line) or as metal hydroxides. The metal ion M^{2+} combines with OH- at the electrode surface to form hydroxide which also diffuses towards the bulk (orange line), so that there is a non-null gradient in the concentration profile of M^{2+} (red line). The bulk gain Y^* is the ratio between the concentrations in the bulk $[M^{2+}]^*$ and at the electrode surface $[M^0]$ (see eqn. (28)). The surface gain Y^S is the ratio between the $[M^0]$ and $[M^{2+}]^S$ (see eqn. (27)).

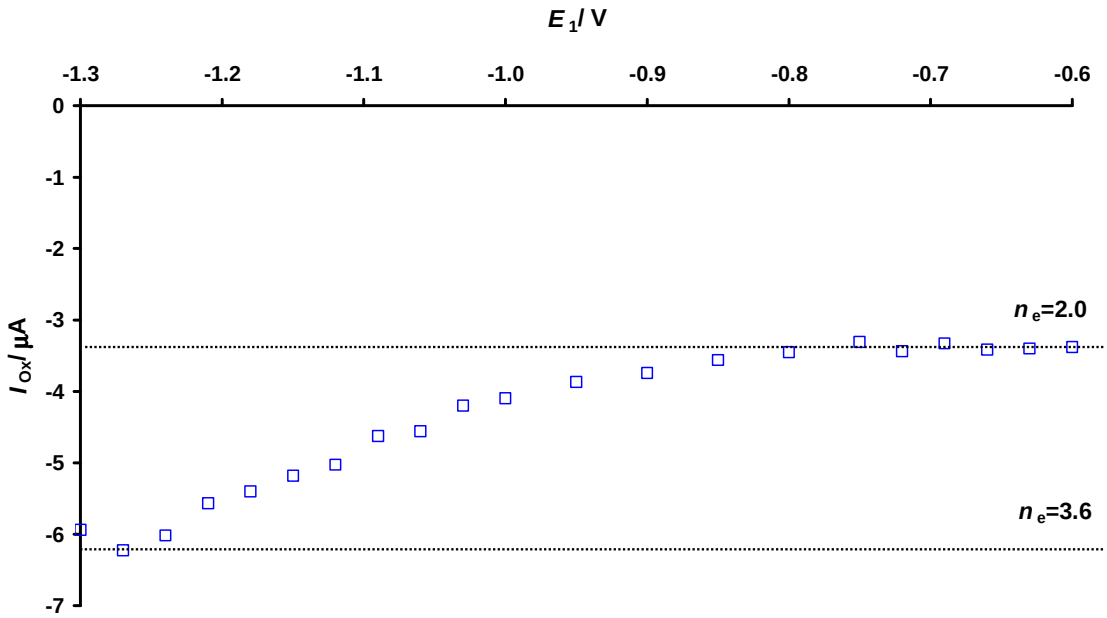

Figure 2. I_{0x} current measured at the end of a deposition stage, for different applied potentials (from -0.60 to -1.30 V, t_1=450 s and t_w=150 s) in a solution with 0.01 M KNO_3, allowing to ascribe the number of electrons transferred in the reduction of oxygen at each potential. n_e=2 has been taken for I_{0x} values measured with potentials more positive than -0.75 V (corresponding to Cd). For Zn (E_1 between -1.05 and -1.16 V), n_e-values between 2.5 and 3.1 have been estimated from the ratio between of I_{0x} values and taking n_e=2 for Cd (see eqn (19) and below).

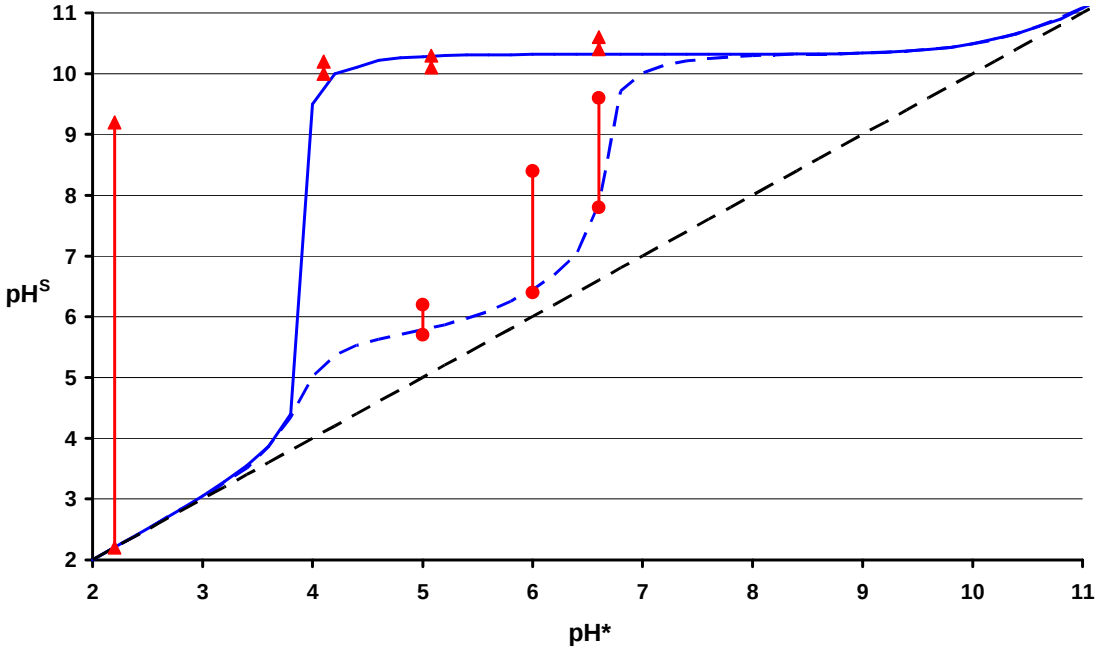

Figure 3. Comparison between the experimental surface pH^S obtained with AGNES (markers) and the theoretical ones computed with the model in non-purged $[Cd^{2+}]$ samples (continuous blue line for non-buffered solutions, discontinuous blue line for samples buffered with [MES]=0.01 M). Dashed black line stands as a reference where pH^S=pH*. The theoretical pH^S have been computed supposing that $2e^-$ are exchanged during the O_2 reduction for the applied deposition potentials. The triangle markers stand for non-buffered samples containing $c_{T,Cd}$=1.5 µM at pH*=2.2, 4.1 or 5.1 (E_1=-0.675 V, t_1=650-1150, t_w=150 s) or $c_{T,Cd}$=1.0 µM at pH*=6.6 ($E_{1,a}$=-1.300 V, $t_{1,a}$=75 s, E_1=-0.705 V, t_w=500 s). The circle markers correspond to solutions with $c_{T,Cd}$=2.5 µM, [MES]=0.01 M, [NTA]= 1.5 µM at pH*=5.0, 6.0 and 6.6 (E_1=-0.675 V, t_1=650-1150, t_w=150 s). The red bars indicate the range of pH^S estimated from Visual Minteq. Large ranges are expected when the Visual Minteq free metal concentration is not significantly affected by pH-changes.

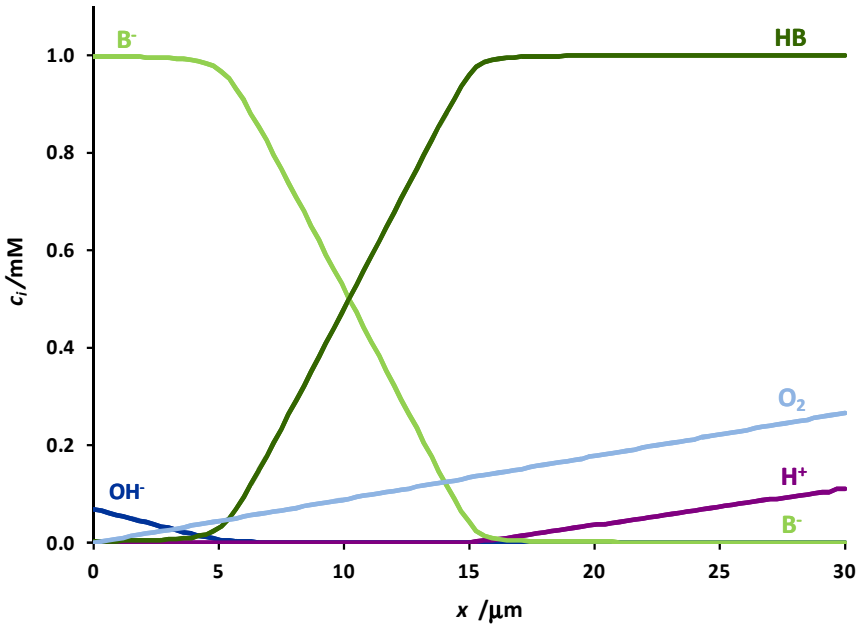

Figure 4: Simulated concentration profiles in a non-purged solution according to the model in section 3. Dark blue line: hydroxide; purple line: proton; light blue line: oxygen; light green line: deprotonated buffer; dark green line: protonated buffer. Parameters: $c^*_{O_2}$ = 2.66 ×10^{-4} M; D_{O_2} =1.97×10^{-9} m^2 s^{-1}; Total buffer concentration= 0.001 M; pK_a of buffer=7.31; Diffusion coefficient of buffer species= 7 ×10^{-10} m^2 s^{-1}; ionic strength=0.01 M; thickness of diffusion layer δ= 30 µm ([13]); n_e=4; pH*=4.

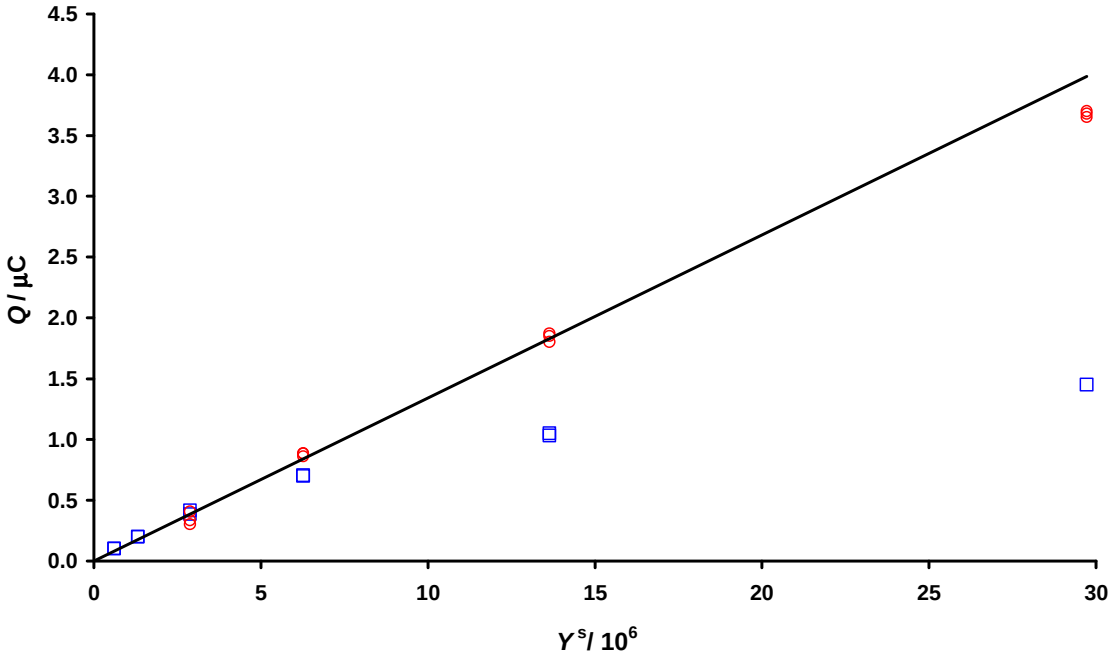

Figure 5: Comparison between the accumulated charges measured with a 1-Pulse AGNES experiment (square markers, E_1 between -1.150 V and -1.190 V and t_1 from 300 to 1650 s and t_w=150 s in a $c_{T,Zn}$=0.76 µM solution at pH*=4.4) or with a 2-Pulses AGNES procedure (circle markers, $E_{1,a}$ =-1.300 V, $t_{1,a}$=30-100 s is optimized for each $E_{1,a}$, $E_{1,b}$ between -1.170 V and -1.190 V, $t_{1,b}$=150-500 s in a $c_{T,Zn}$=0.76 µM solution at pH*=4.35) in a non-purged solution. 2-Pulses AGNES allows obtaining a good linearity between Q and Y^S (see the reference black line which shows the theoretical Q vs Y^S expected behaviour if steady state was achieved in all the studied gains). Underestimated values can be obtained with 1-Pulse AGNES when unsufficiently long deposition times are applied for huge Y^S gains.

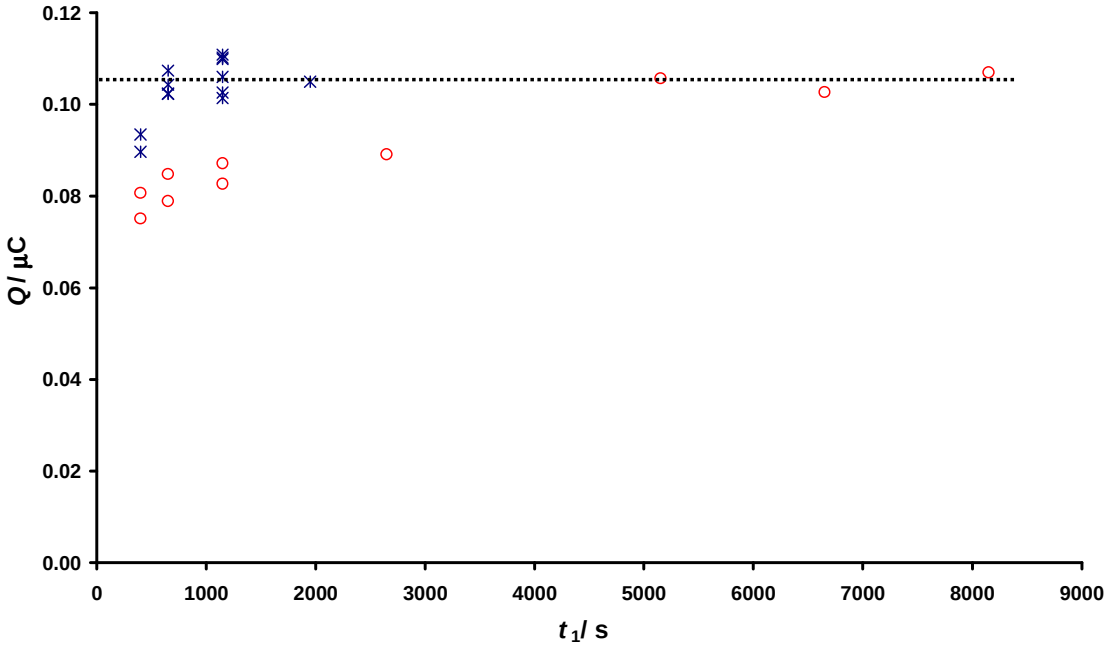

Figure 6: Measured faradaic charges in a 1-Pulse AGNES experiment with a stirred (* markers) or unstirred (○ markers) accumulation stage at different deposition times (t_1) and t_w=150s. Parameters: $c_{T,Zn}$=1.25 µM, pH*= 4.35, E_1=-1.160 V.

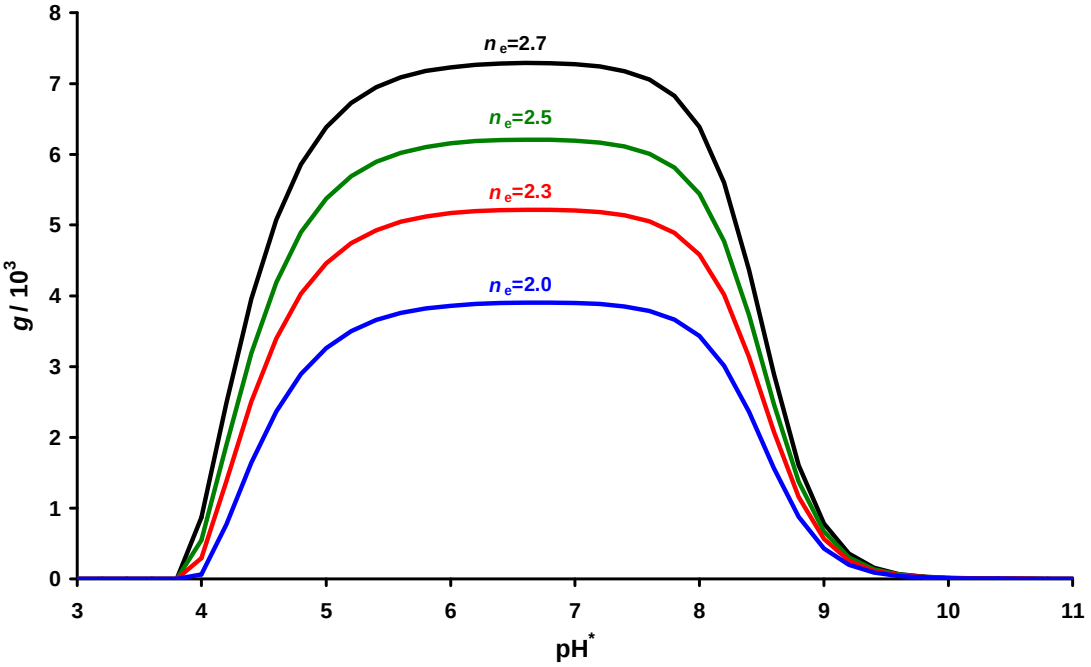

Figure 7: Interference of the dissolved oxygen expressed as g and computed with eqn. (36) in a solution with $c_{T,Zn}$=1.5 µM at different pH* and different number of electrons exchanged: 2.0 (blue line), 2.3 (red line), 2.5 (green line) and 2.7 (black line).

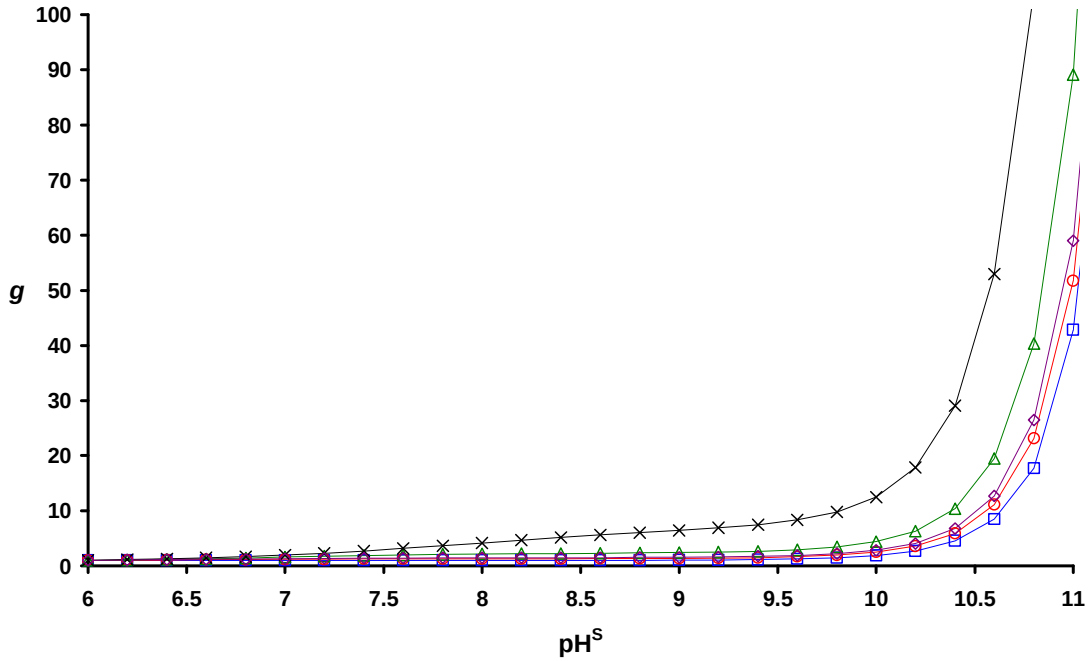

Figure 8: Impact of surface pH on the *g* values, computed with Visual Minteq, in a solution with $c_{T,Cd}$=0.3 µM, [NTA] = 0 µM (□ markers), 0.10 µM (○ markers), 0.13 µM (◊ markers), 0.20 µM (Δ markers) and 0.26 µM (× markers) at pH*=6.0 (non-buffered).

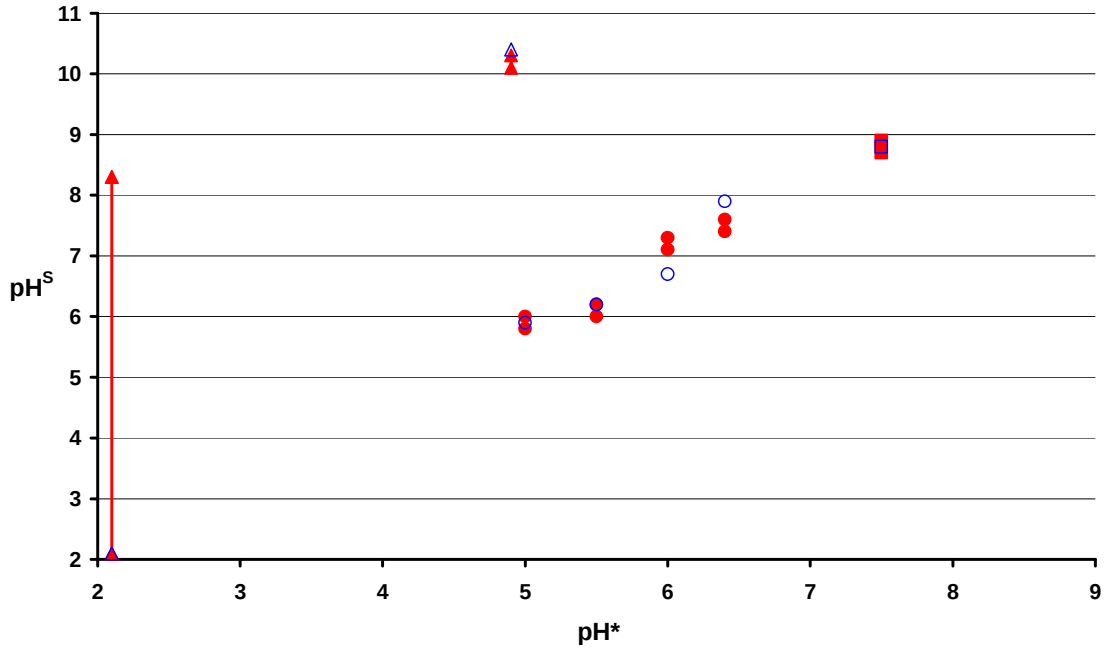

Figure 9: Experimental (full markers) and theoretical (empty markers) pH^S estimated in non-purged [Zn^{2+}] solutions at different bulk pH*. The triangle markers represent the experiments performed in a non-buffered solution with $c_{T,Zn}$=1.5 µM at pH*=2.1 (E_1=-1.055 V and t_1 between 650 and 1150 s and t_w =150 s) and pH*=4.9 (E_1=-1.160 V, t_1 between 650 and 1150 s and t_w =150 s). The circle markers stand for solutions containing $c_{T,Zn}$=1.5 µM, [MES]=0.01 M, [NTA]=1.5 µM at pH*=5.0, 5.5, 6.0 and 6.4 (E_1 between -1.080 V and -1.100 V with t_1 from 650 to 1150 s and t_w =150 s). The square markers correspond to a sample with $c_{T,Zn}$=1.0 µM, [MOPS]=0.01 M, [glycine]= 200 µM at pH*=7.6 (E_1=-1.110 V and t_1=650 s and t_w =150 s). The red bars correspond to the pH^S range where the metal speciation, for the corresponding sample composition, does not change practically.

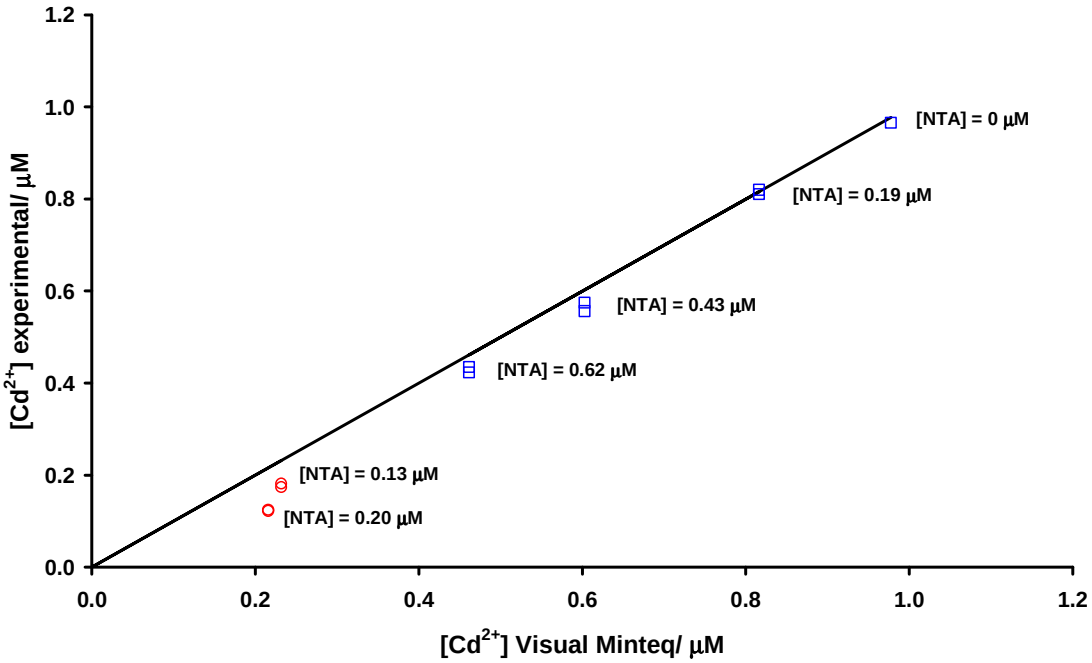

Figure 10: Determination of free Cd^{2+} in a sample with: i) $c_{T,Cd}$=0.3 µM with NTA 0.13 and 0.20 µM at pH*=6.0 represented (red circles). AGNES conditions were E_1=-0.711 V, t_1 between 1400 and 1750 s and t_w =150 s; ii) $c_{T,Cd}$=1.0 µM, [MES]=0.01 M and NTA from 0.19 to 0.62 µM at pH*=6.7 (blue squares). AGNES conditions were E_1=-0.675 V, t_1 between 650 and 1150 s and t_w =150 s. The continuous line stands for the theoretical free Cd^{2+} concentration estimated with Visual Minteq.

9. 1 **P. Delahay, *New Instrumental Methods in Electrochemistry*, Interscience, New York, 1954.**

10. 2 **C. M. Sánchez-Sánchez, J. Rodríguez-López, A. J. Bard, *Anal.Chem.* 2008, 80, 3254-3260.**

11. 3 **R. Reinke, J. SIMON, *Anal.Bioanal.Chem.* 2002, 374, 1256-1260.**

12. 4 **J. Buffle, M. Spoerri, *J.Electroanal.Chem.* 1981, 129, 67-88.**

13. 5 **V. N. Statsyuk, M. B. Dergacheva, *Russ.J.Gen.Chem.* 1998, 68, 691-693.**

14. 6 **Y. N. Antonenko, P. Pohl, *BBA-Biomembranes* 1995, 1235, 57-61.**

15. 7 **B. R. Horrocks, M. V. Mirkin, D. T. Pierce, A. J. Bard, G. Nagy, K. Toth, *Anal.Chem.* 1993, 65, 1213-1224.**

16. 8 **M. L. Tercier-Waeber, J. Buffle, *Environ.Sci.Technol.* 2000, 34, 4018-4024.**

17. 9 **E. M. Richter, J. J. Pedrotti, L. Angnes, *Electroanal.* 2003, 15, 1871-1877.**

18. 10 **K. A. Howell, E. P. Achterberg, C. B. Braungardt, A. D. Tappin, D. R. Turner, P. J. Worsfold, *Analyst.* 2003, 128, 734-741.**

19. 11 **K. Gibbon-Walsh, P. Salaün, C. M. G. van den Berg, *J.Phys.Chem.A* 2012, 116, 6609-6620.**

20. 12 **O. A. Farghaly, *Microchemical Journal* 2003, 75, 119-131.**

21. 13 **C. Parat, A. Schneider, A. Castetbon, M. Potin-Gautier, *Anal.Chim.Acta* 2011, 688, 156-162.**

22. 14 **G. Alberti, R. Biesuz, C. Huidobro, E. Companys, J. Puy, J. Galceran, *Anal.Chim.Acta* 2007, 599, 41-50.**

23. 15 **C. Huidobro, E. Companys, J. Puy, J. Galceran, J. P. Pinheiro, *J.Electroanal.Chem.* 2007, 606, 134-140.**

24. 16 **R. F. Domingos, C. Huidobro, E. Companys, J. Galceran, J. Puy, J. P. Pinheiro, *J.Electroanal.Chem.* 2008, 617, 141-148.**

25. 17 **J. P. Pinheiro, J. Salvador, E. Companys, J. Galceran, J. Puy, *Phys.Chem.Chem.Phys.* 2010, 12, 1131-1138.**

26. 18 **L. S. Rocha, E. Companys, J. Galceran, H. M. Carapuca, J. P. Pinheiro, *Talanta* 2010, 80, 1881-1887.**

27. 19 **D. Chito, J. Galceran, E. Companys, *Electroanal.* 2010, 22, 2024-2033.**

28. 20 **D. Aguilar, C. Parat, J. Galceran, E. Companys, J. Puy, L. Authier, M. Potin-Gautier, *J.Electroanal.Chem.* 2013, 689, 276-283.**

29. 21 **C. Parat, D. Aguilar, L. Authier, M. Potin-Gautier, E. Companys, J. Puy, J. Galceran, *Electroanal.* 2011, 23, 619-627.**

30. 22 C. Parat, L. Authier, D. Aguilar, E. Companys, J. Puy, J. Galceran, M. Potin-Gautier, *Analyst.* 2011, 136, 4337-4343.

31. 23 D. Chito, J. Galceran, E. Companys, J. Puy, *J.Agric.Food Chem.* 2013, 61, 1051-1059.

32. 24 E. Companys, M. Naval-Sanchez, N. Martinez-Micaelo, J. Puy, J. Galceran, *J.Agric.Food Chem.* 2008, 56, 8296-8302.

33. 25 B. Pernet-Coudrier, E. Companys, J. Galceran, M. Morey, J. M. Mouchel, J. Puy, N. Ruiz, G. Varrault, *Geochim.Cosmochim.Ac.* 2011, 75, 4005-4019.

34. 26 E. Companys, J. Puy, J. Galceran, *Environ.Chem.* 2007, 4, 347-354.

35. 27 C. David, J. Galceran, C. Rey-Castro, J. Puy, E. Companys, J. Salvador, J. Monné, R. Wallace, A. Vakourov, *J.Phys.Chem.C* 2012, 116, 11758-11767.

36. 28 R. F. Domingos, D. F. Simon, C. Hauser, K. J. Wilkinson, *Environ.Sci.Technol.* 2011, 45, 7664-7669.

37. 29 J. Galceran, C. Huidobro, E. Companys, G. Alberti, *Talanta* 2007, 71, 1795-1803.

38. 30 F. Zavarise, E. Companys, J. Galceran, G. Alberti, A. Profumo, *Anal.Bioanal.Chem.* 2010, 397, 389-394.

39. 31 J. Galceran, E. Companys, J. Puy, J. Cecília, J. L. Garcés, *J.Electroanal.Chem.* 2004, 566, 95-109.

40. 32 E. Companys, J. Cecília, G. Codina, J. Puy, J. Galceran, *J.Electroanal.Chem.* 2005, 576, 21-32.

41. 33 J. Galceran, D. Chito, N. Martinez-Micaelo, E. Companys, C. David, J. Puy, *J.Electroanal.Chem.* 2010, 638, 131-142.

42. 34 D. Jagner, *Analyst.* 1982, 107, 593-599.

43. 35 R. M. Town, H. P. van Leeuwen, *J.Electroanal.Chem.* 2001, 509, 58-65.

44. 36 R. M. Town, H. P. van Leeuwen, *Electroanal.* 2004, 16, 458-471.

45. 37 C. Parat, L. Authier, S. Betelu, N. Petrucciani, M. Potin-Gautier, *Electroanal.* 2007, 19, 403-406.

46. 38 D. R. Lide, *CRC Handbook of Chemistry and Physics*, 77 ed. CRC Press, Boca Raton, FA, 1996.

47. 39 D. Jagner, *Anal.Chem.* 1979, 51, 342-345.

48. 40 M. Pelletier, J. Buffle, D. Monnier, *Chimica* 1973, 25, 61.

49. 41 M. Auinger, I. Katsounaros, J. C. Meier, S. O. Klemm, P. U. Biedermann, A. A. Topalov, M. Rohwerder, K. J. J. Mayrhofer, *Phys.Chem.Chem.Phys.* 2011, 13, 16384-16394.

50. 42 J. Galceran, S. L. Taylor, P. N. Bartlett, *J.Electroanal.Chem.* 2001, 506, 65-81.

51. 43 A. Molina, J. Gonzalez, E. Laborda, Y. J. Wang, R. G. Compton, *Phys.Chem.Chem.Phys.* 2011, 13, 14694-14704.

52. 44 J. Galceran, J. Puy, J. Salvador, J. Cecília, F. Mas, J. L. Garcés, *Phys.Chem.Chem.Phys.* 2003, 5, 5091-5100.

53. 45 J. Puy, R. Uribe, S. Mongin, J. Galceran, J. Cecilia, J. Levy, H. Zhang, W. Davison, *J.Phys.Chem.A* 2012, 116, 6564-6573.

54. 46 S. Wolfram, *Mathematica 9. A System for Doing Mathematics by Computer*, Addison-Wesley Publishing Company, Redwood City (California), 2012.

55. 47 R. M. Town, H. P. van Leeuwen, *J.Electroanal.Chem.* 2001, 515, 129.

56. 48 J. Buffle, *J.Electroanal.Chem.* 1981, 125, 273-294.

57.